

Modeling the temperature-rise behavior of 2D triaxial braided composites under impact loads

Chao Zhang^{1,2,3}, Peng Liu^{2,3}, Yulong Li^{1,2,3}

¹School of Aeronautics, Northwestern Polytechnical University, Xi'an, Shaanxi 710072, China ²School of Civil Aviation, Northwestern Polytechnical University, Xi'an, Shaanxi 710072, China ³Joint International Research Laboratory of Impact Dynamics and Its Engineering Application, Xi'an, Shaanxi 710072, China

Abstract

Due to their special geometric structure, the damage evolution and crack propagation behavior of twodimensional triaxially braided composite (2DTBC) is complicated and unique. In addition, under high-speed impact loads, the adiabatic heating-induced temperature rise may cause a phase change in the resin material. Therefore, the damage and failure behavior of 2DTBC under impact load is considered to be a dynamic and thermo-mechanical coupled problem. It is then necessary to develop an appropriate numerical method that is able to capture the temperature rise behavior of 2DTBC under various loading conditions. This study introduces infrared thermal imaging, quasi-static, low-velocity impact, and high-speed impact tests to measure the thermal response of the material during different loading conditions. Through the comparison against geometric configuration and full-field strain distribution images, the correlation between temperature-rise behavior with deformation and damage are systematically analyzed. An elastoplastic progressive damage constitutive model for fiber bundle was established with consideration of strain-rate dependency and thermal-mechanical coupling. A meso-scale finite element (FE) model for 2DTBC was developed to model the quasi-static and impact failure behaviors. Combing the experimental and simulation results, the temperature-rise behavior was clarified and the rate-dependent damage mechanism was revealed. The accuracy and applicability of the FE model were validated. The research results can provide theoretical basis and modeling tool for the practical application of this type of composites.

Keywords: Triaxially braided composite; high-speed impact load; meso-scale FE; temperature rise;

1. Introduction

Braided composite materials have gained widespread adoption in the manufacturing of structural components for aircraft and engines in recent years, owing to their easy molding process, superior damage resistance [1], and enhanced anti-delamination characteristics when compared to conventional laminated panels [2]. With their increasing application in impact protection, the impact resistance of braided composites has garnered attention. Observations indicate that these materials undergo significant temperature increases when subjected to impact loads, a phenomenon intricately linked to their impact resistance capabilities. However, the underlying mechanism of this temperature rise in composite materials remains poorly understood, and the implications of such thermal effects on their mechanical properties are yet to be fully understood.

Numerous studies have utilized infrared thermography to analyze the damage behavior of composite materials, monitoring temperature variations on the surfaces of test specimens. Yu et al. [3] utilized an infrared camera to track temperature changes on the surface of tensile specimens under quasistatic loading conditions. They discovered a correlation between the areas displaying temperature increases as detected by infrared thermography and damage zones within the composite material.

Tuo et al. [4] investigated damage behavior in composite materials due to low-velocity impacts and subsequent compression, concluding that the thermal field could effectively demonstrate the initiation of damage. Zhao et al. found that localized temperature spikes in specimens might indicate different damage modes in epoxy resin composite laminates. In a detailed observation of the low-velocity impact test procedure, Maierhofer et al. [5] employed an infrared camera. Their results indicated that thermal imaging could successfully differentiate between various damage types and possibly monitor crack progression. However, it's worth noting that despite the capability to capture temperature rise phenomena during quasi-static and low-speed impact tests experimentally, the temperature increase is typically below 30°C, which is not likely to significantly influence the material's overall performance. Under high-speed impact conditions, composite materials may experience significant temperature elevations, with the peak temperature potentially reaching 200°C [6], which could exceed the resin's glass transition temperature and significantly alter the material's mechanical properties and failure modes. Pan et al. [7,8] utilized high-speed infrared cameras combined with Split Hopkinson Pressure Bar (SPHB) techniques to investigate the dynamic failure behavior of three-dimensional braided composites, revealing a relationship between localized surface temperature spikes and internal damage mechanisms. Li et al. [9] observed a linear relationship between the temperature rise rate and the rate of loading during dynamic tensile-compressive experimentation on carbon fiber/epoxy composites. Pournoori and coworkers [10,11] identified the initiation and evolution of damage as key factors leading to temperature increases during dynamic compression tests on glass and carbon fiber-reinforced composites. Papantonakis et al. [12] noted that the extent of temperature elevation in composite plates widens as impact velocity increases. Moreover, Marcotte and others [13] pointed out that in cases where composite targets are not breached, the dissipated thermal energy during high-speed impacts can be equivalent to half of the projectile's kinetic energy. While current research has harnessed the phenomenon of temperature rise as a damage indicator, relying solely on infrared cameras to monitor surface temperature fluctuations is insufficient for accurately determining temperature-dependent damage mechanisms. Thus, high-precision finite element modeling techniques are imperative for the in-depth exploration of temperature-induced failure behaviors in composite materials.

Pan et al. [14-15] crafted a thermo-mechanical constitutive model for composite materials that demonstrated how localized temperature spikes in composites are generated from the conversion of plastic deformation work into heat. The model's simulated temperature field distribution accurately aligned with the regions identified as damaged. Building upon this development, Zhang [16] factored in the strain rate response and thermal effects into the constitutional modeling for composite materials. Simulations of dynamic compression on 3D braided composites at various strain rates revealed shear failure as the predominant form of breakdown, with a pronounced correlation between temperature and stress distributions and the regions of damage. Chen [17] probed the thermal behavior under combined shear and compression loading in 3D braided composites via a microscale approach. Results showed that transient thermal accumulation in the resin matrix, largely resulting from shearcompression forces, notably hastened shear band failure. Collectively, these research contributions assert that the plastic work and fracture energies released during a material's failure phase are chief sources of the resultant temperature rise. However, microscopic finite element simulations that address temperature responses to impact in woven composites face limitations due to high computational demands. Thus, the pursuit of effective mesoscale finite element impact models and highly accurate strain rate-sensitive thermo-mechanical constitutive models continues to stand as a significant challenge in the field.

To precisely delineate the relationship between temperature elevation and damage deformation in braided composite materials, our study executed a series of quasi-static, low-velocity impact, and high-speed impact simulation experiments to capture thermal response data. We formulated constitutive models that account for rate-dependent and temperature-dependent effects, addressing both anisotropic elastoplastic progressive damage in fiber bundles and isotropic elastoplastic damage in the matrix. We also established efficient and high-fidelity mesoscopic finite element models tailored

for comprehensive analysis of large-scale specimen impact failures. Through quasi-static, low-velocity impact, and high-speed impact simulation analyses, complemented by experimental validation, we confirmed the precision and practicality of our models. By rigorously considering the individual elements of woven composites, including fiber bundles, resin, and interfaces, our study yielded highly accurate damage failure predictions. This work illuminates the failure behaviors and thermal effects in 2D triaxial braided composites under various loading conditions. Furthermore, we elucidated the interplay between mechanical reactions and temperature escalation, uncovering the origins of temperature rise during impact and its subsequent impact on the mechanical integrity of 2D triaxial braided composites.

2. Experiments

This study elaborates on the fabrication of 2D Triaxial Braided Composite (2DTBC) plates using T700 carbon fibers and 3266 epoxy resin through the Resin Transfer Molding (RTM) process. The finished composite plates, comprised of eight layers, feature an average thickness of 4.56mm and a consistent fiber volume fraction of 56%. The properties of both the fiber bundles and the epoxy resin are referenced from manufacturer data and validated by existing literature [18], while microscopic analysis of the cross-sections confirms a fiber volume fraction within the bundles of approximately 71.4%.

The quasi-static tensile testing of the 2DTBC was meticulously conducted by ASTM D3039 and ASTM D3410 standards, employing a 200 kN PLD 250 electro-hydraulic servo testing machine, as depicted in Figure 1. The displacement fields were accurately measured using speckle patterns captured by a Daheng Optics MER-2000-19U3M/C camera, equipped with Digital Image Correlation (DIC) technology. The strain along the load direction was precisely assessed on the composite's reverse side. Strain fields derived from DIC were averaged and cross-verified with strain gauge data for accuracy. A FLIR-A655SC infrared camera, positioned alongside the optical camera, was tasked with monitoring the surface temperature fields. This setup provided a broad temperature measurement range from -40°C to 650°C, with an accuracy of ±2°C, at a resolution of 640×480 pixels and a frame rate of 50 Hz. The infrared data was outputted via an RJ45 connection to software, enabling real-time temperature tracking. For the duration of the tensile tests, the load speed was maintained at a constant 8.4 mm/min until failure occurred, with both the testing machinery and strain gauges collecting data at a rate of 2 Hz.

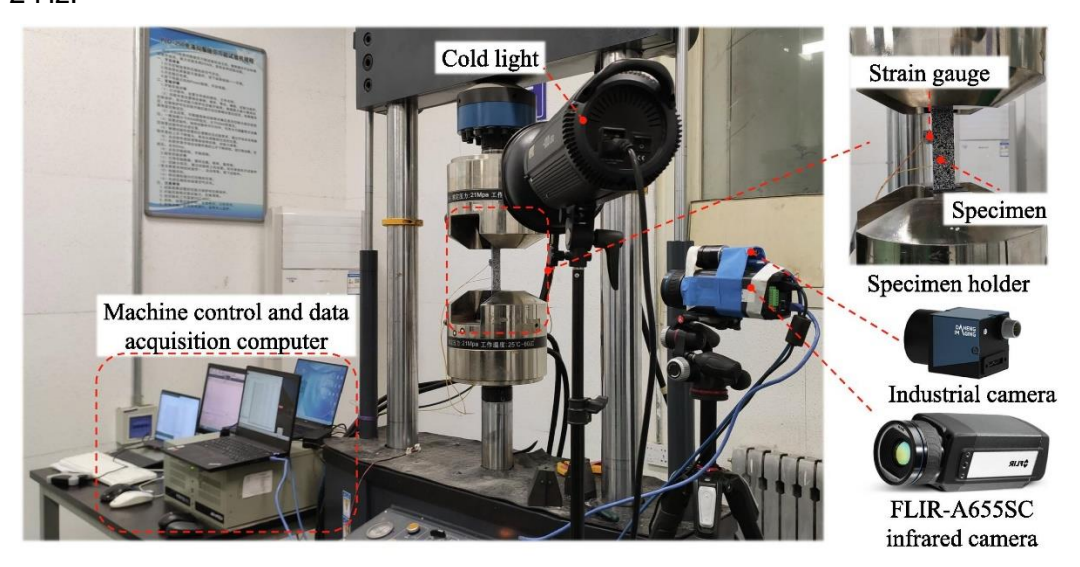


Figure 1 – Experimental setup of the quasi-static test;

The low-velocity impact testing of 2DTBC is carried out in strict adherence to the ASTM D-7136 standard [19]. Figure 2 showcases the experimental setup designated for this low-velocity impact test. The testing process is conducted employing an Instron 9250HV drop-weight impact testing machine, which comes equipped with a mechanism designed to prevent secondary impacts. The impactor consists of a hemispherical steel head with an 8 mm radius, connected to a rear mass block that

facilitates weight adjustment by adding or removing masses. For this study, a total mass of 5.71 kg is employed. The specimen is securely positioned within a frame fixture underneath the impactor, featuring a central opening measuring 125 mm \times 75 mm. Four rubber heads are utilized to constrain the specimen's out-of-plane displacement. Before testing, the impactor is raised to a predetermined height and then released to impact the specimen. The impactor height is adjusted to achieve the desired impact energy.

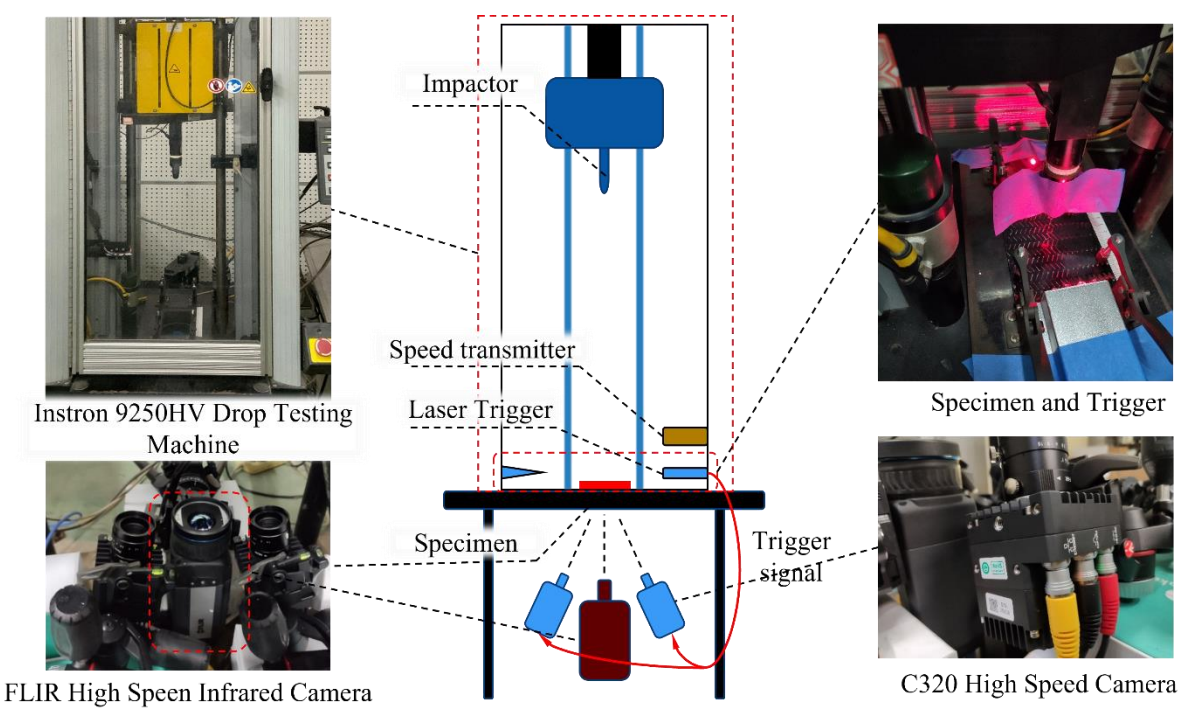


Figure 2 – Experimental setup of the low-velocity impact test setup;

High-velocity impact testing on 2DTBC adhered to ASTM D8101, utilizing a 50mm×50mm×6mm titanium alloy projectile enclosed within a 3D-printed sabot in a guided barrel, ensuring non-rotational travel, as depicted in Figure 3. The sabot was propelled by high-pressure gas and released at the barrel's end, with the target positioned approximately 1m away to maintain projectile orientation upon impact. The target, secured by screws and clamps, provided a 200 mm×200 mm inspection area. For deformation analysis, a 3D Digital Image Correlation (DIC) system, comprising a pair of Phantom 1310 high-speed cameras and ARAMIS 3D software, recorded at 800×600 resolution and 24,000 Hz. A Phantom C320 camera captured side impact footage at 1280×720 resolution and 10,000 Hz, facilitating projectile velocity measurement using a scale ruler for spatial calibration. The same camera, with a 0.1 ms inter-frame interval, enabled velocity determination through frame-by-frame comparison. Another Phantom C320 recorded the impact angle at 640×304 resolution and 5,100 Hz. A FLIR X6520sc infrared camera measured backside temperature fields during impact. Cameras positioned behind the target were equipped with protective shielding.

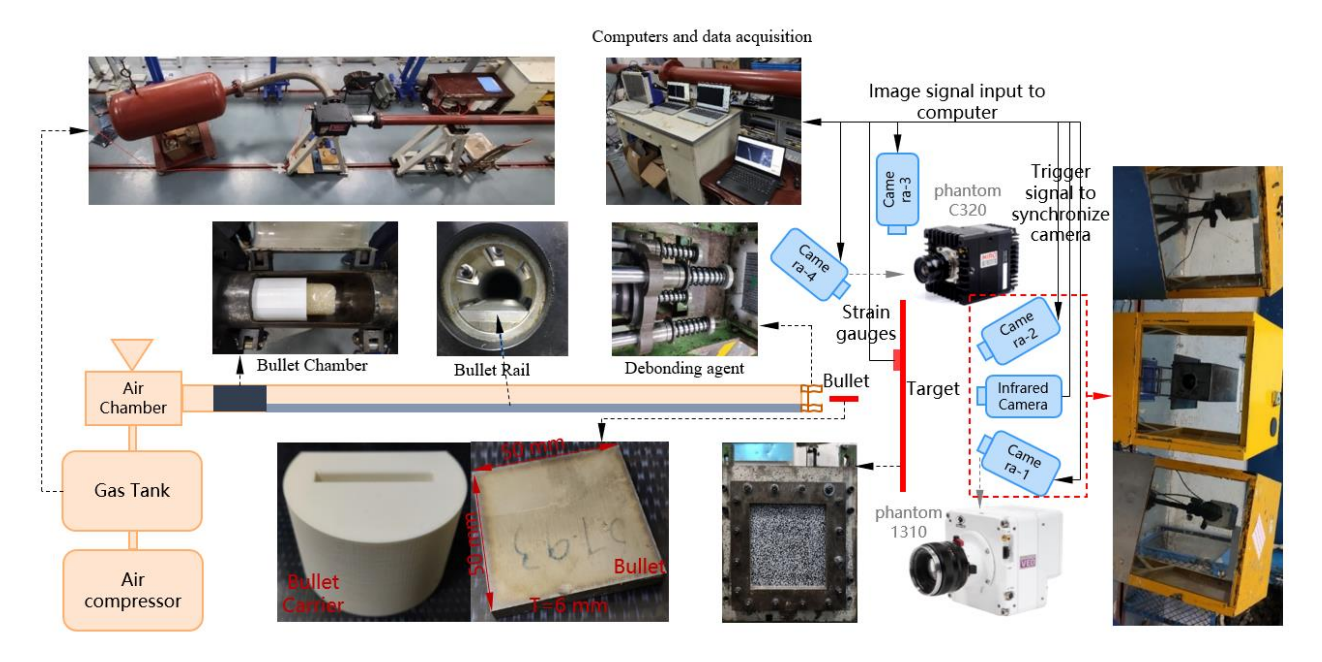


Figure 3 – Experimental setup of the high-speed impact test setup;

3. Thermal-mechanical coupled constitutive model of fiber bundles and pure matrix

The primary drivers of temperature rise in composite materials are the plastic work and fracture energy dissipated by both the matrix and fiber bundles. To accurately capture the behavior of 2DTBC under impact loading, we developed elastoplastic progressive damage constitutive models for the matrix and fiber bundles. These models translate the plastic work and fracture energy released during material deformation into thermal energy. Furthermore, we incorporated rate-dependent and thermal effects into the composite material's constitutive response to account for the influence of strain rate and temperature on the material's mechanical properties.

Fiber bundles are considered transversely isotropic materials, and the relationship between plastic work, fracture energy, and thermal energy conversion is established based on the Hill anisotropic yield criterion. The plastic potential function for Hill's yield criterion can be expressed as:

$$f(\sigma) = \sigma_{\rm H} = \sqrt{\{\sigma\}[H]\{\sigma\}^{\rm T}} = \sqrt{F(\sigma_{22} - \sigma_{33})^2 + G(\sigma_{33} - \sigma_{11})^2 + H(\sigma_{11} - \sigma_{22})^2 + 2L\sigma_{23}^2 + 2M\sigma_{31}^2 + 2N\sigma_{12}^2}$$
(1)

In equation (1), F, G, H, L, M, and N represent the anisotropic characteristic parameters of the material, which are detailed in reference [20]. The fiber bundle damage model in this study employs the Hashin-Hou damage criterion, which encompasses four damage modes:

Fiber tension damage $(\sigma_{11}>0)$:

$$e_{\text{ft}} = \left(\frac{\sigma_{11}}{F_{1t}}\right)^2 + \alpha \left(\frac{\sigma_{12}^2 + \sigma_{13}^2}{F_{\text{ls}}}\right) \ge 1$$
 (2)

Fiber compression damage (σ_{11} <0):

$$e_{fc} = \left(\frac{\sigma_{11}}{F_{1c}}\right)^2 \ge 1 \tag{3}$$

Matrix tension damage $(\sigma_{22}>0)$:

$$e_{\text{mt}} = \left(\frac{\sigma_{22}}{F_{2t}}\right)^2 + \left(\frac{\sigma_{12}}{F_{\text{ls}}}\right)^2 + \left(\frac{\sigma_{23}}{F_{\text{ts}}}\right)^2 \ge 1 \tag{4}$$

Matrix compressive damage (σ_{22} <0):

$$e_{\text{mc}} = \frac{1}{4} \left(\frac{-\sigma_{22}}{F_{ls}} \right)^2 + \frac{F_{2c}^2 \sigma_{22}}{4F_{ls}^2 F_{2c}} - \frac{\sigma_{22}}{F_{2c}} + \left(\frac{\sigma_{12}}{F_{ts}} \right)^2 \ge 1$$
 (5)

In equations (2) to (5): e_{ft} , e_{fc} , e_{mt} and e_{mc} represent the damage indices for the four distinct modes of damage. When these indices reach or exceed a value of 1, it indicates the onset of the corresponding damage mode in the material. F_{1t} , F_{1c} , F_{2t} , F_{2c} , F_{1s} and F_{ts} respectively denote the tensile strength in the axial direction of the fiber bundles, axial compression strength, transverse tensile strength, transverse compression strength, longitudinal shear strength, and transverse shear strength. The variables σ_{11} , σ_{22} , σ_{12} , σ_{13} and σ_{23} respectively represent the stresses on the fiber bundles in their respective directions. Within equation (2), the parameter σ_{11} serves as a shear factor, quantifying the contribution of shear stress to tensile damage in fibers.

Based on the plastic and damage responses of the fiber bundles, the plastic work and fracture energy of the unit can be computed, and from there, the temperature rise can be determined by the principle of energy conservation. The method for calculating plastic work is:

$$\Delta \mathsf{W}^{\mathsf{pl}} = \left\{ \sigma \right\} \Delta \left\{ \varepsilon \right\}^{\mathsf{pl}} \tag{6}$$

In equation (6), ΔW^{pl} represents the increment of plastic work, and $\{\sigma\}$ and $\{\sigma\}$ are consistent with previously introduced terms. The method for calculating the temperature rise from plastic work is:

$$\beta_{\rm pl}\Delta W^{\rm pl} = \rho C \Delta T \tag{7}$$

Where ρ , C, β_{pl} and ΔT respectively denote the density of the fiber bundle, specific heat capacity, the thermomechanical conversion coefficient of plastic work, and the resultant temperature rise. This study focuses on the temperature rise behavior of 2DTBC under impact loads, it is imperative to consider the strain rate effects of the fiber bundles. The rate and thermal effects in this research are referenced using the Johnson-Cook (*J-C*) constitutive model. The relationship between stress, strain rate, and temperature can be expressed as follows:

$$\bar{\sigma}_{\dot{\varepsilon}T} = \left(\sigma_{y_0} + R(\bar{\varepsilon}^{pl})\right) (1 + C \ln \frac{\dot{\bar{\varepsilon}}}{\dot{\bar{\varepsilon}}_0}) (1 - \left(\frac{T - T_r}{T_m - T_r}\right)^m)$$
(8)

Where $\left(\sigma_{y_0} + R(\bar{\varepsilon}^{\rm pl})\right)$ represents the material's equivalent plastic stress-strain data under quasistatic loading conditions, C and m are the material's strain rate sensitivity coefficient and temperature softening coefficient, respectively, which require calibration based on existing literature and denote the current equivalent plastic strain rate and the reference equivalent plastic strain rate, respectively, T_{N} , T_{P} and T_{P} represent the material's temperature, room temperature, and melting temperature. To provide a better understanding of the proposed constitutive model, the elastoplastic and damage behavior in the shear direction is shown in Figure 4. The behavior can be divided into three phases: a purely elastic phase, a plastic phase, and a damage phase. Once the plastic response is obtained, the temperature rise will be calculated from the plastic work using Equation (7).

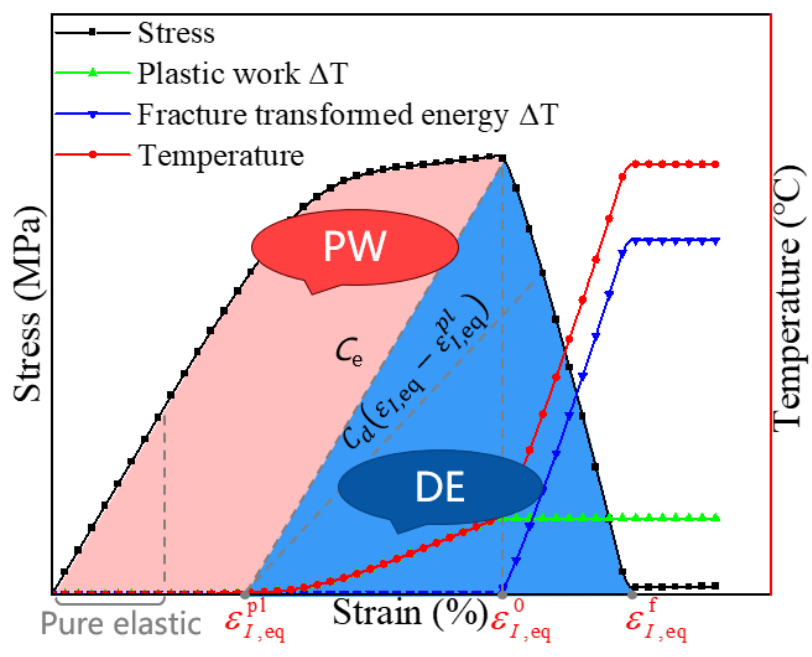


Figure 4 – Mechanical-thermal response for fiber tows;

4. Model Validation

Figure 5(a) depicts the comprehensive stress-strain curve along with the corresponding strain cloud diagrams obtained from both quasi-static tensile tests and simulations. The shaded region within the stress-strain curve demonstrates the repeatability observed across three individual tests. In contrast, the simulated curve is formulated based on the ratio of displacement at the reference point and the applied load to the specimen's initial length and cross-sectional area. Both the simulation and test results exhibit highly correlated strain cloud diagrams. Notably, the absence of a pure matrix layer on the exterior surface of the simulation model results in a strain cloud diagram with more pronounced contours compared to the test diagram. The close alignment between the simulated and experimental stress-strain curves, as well as the strain cloud diagrams, substantiates the effectiveness and accuracy of the mesoscale finite element analysis.

The comparison between temperature fields captured by an infrared camera during axial tensile tests and those predicted by simulations identifies a localized maximum temperature near 50° C at the point of sample failure, primarily concentrated around the $0^{\circ}/\pm60^{\circ}$ braided fiber bundles. Furthermore, Figure 5(b) illustrates the comprehensive temperature rise (ΔT), including the contributions from plastic work and fracture energy, for both axial and bias fiber bundles in the simulation. The temperature rise in axial fiber bundles is primarily attributed to fracture energy, consistent with the observed fiber tension damage shown in Figure 5(b). Conversely, the temperature rise in bias fiber bundles, resulting from plastic work and fracture energy, is minimal and does not match their overall temperature profiles. Therefore, the temperature rise in bias bundles is predominantly due to thermal conduction from nearby axial bundles, which corroborates the locations of fiber tension damage in the axial bundles.

Comparing axial and transverse tensile conditions reveals that matrix tension damage results in only a minor temperature increase. Under axial tension, specimen failure triggers significant delamination damage, with interlaminar interface damage within fiber bundles proving more critical than damage between layers. Experimental observations show notable temperature rises in the central region of the specimen along paths perpendicular to the loading direction under both transverse and axial tension, as depicted in Figure 5(c). This phenomenon is even more pronounced in simulations, where, similar to axial tension scenarios, the temperature rise (ΔT) in transverse tension specimens mainly stems from the conversion of fracture energy due to fiber breakage in bias bundles. Analysis of damage morphology in experimental specimens and simulated damage patterns indicate that axial

fiber bundles undergo matrix cracking, which does not markedly impact the temperature in the affected area. This minimal temperature effect is attributed to the relatively low stress experienced by axial fiber bundles in the perpendicular direction, which inhibits significant strain energy accumulation.

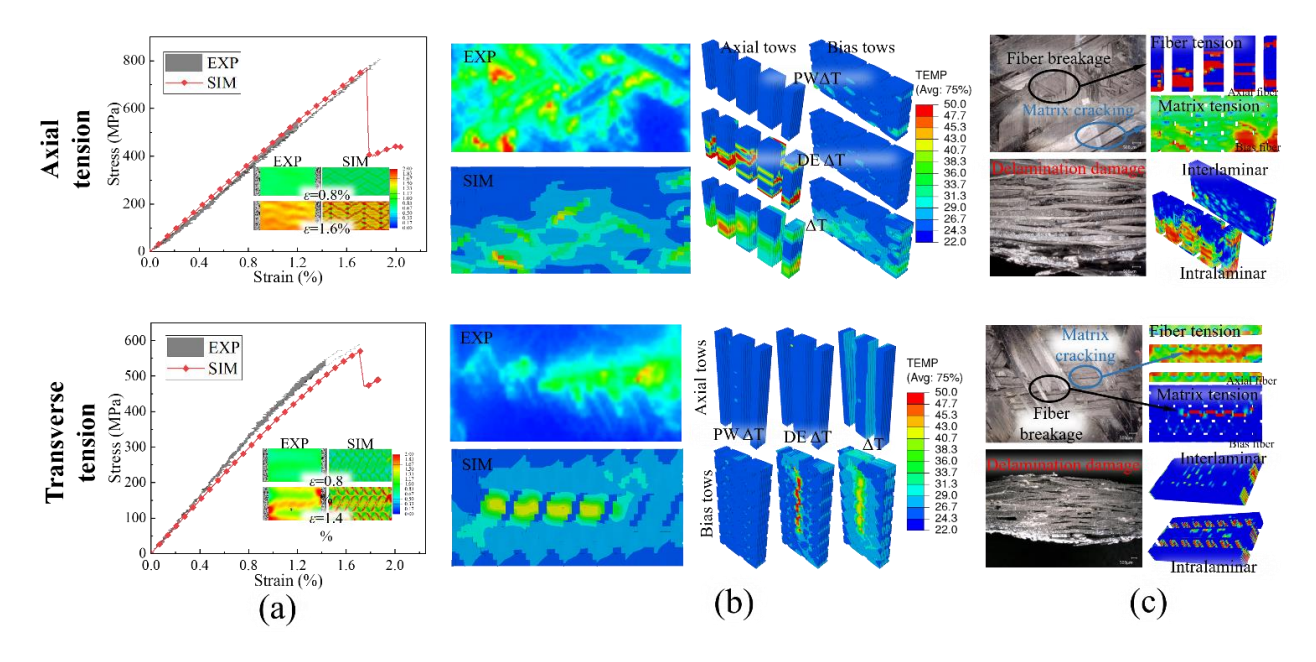


Figure 5 – Temperature and damage contours under tensile load: (a) stress-strain response for axial and transverse directions; (b) comparison of temperature rise phenomena between experimental result and FE simulation; (c) comparison of failure Modes between experimental result and FE simulation;

Figure 6(a) demonstrates a high degree of consistency between experimental data and simulation results, including aspects such as the initial contact response, maximum impact force and displacement, rebound response, residual deformation, and energy absorption. This consistency suggests that the established low-velocity impact model can accurately simulate the overall mechanical response of 2DTBC under low-velocity impact conditions. Figure 6(b) compares the outof-plane displacement contour maps at the impact point on the backside of the specimen between experiments and simulations. The legend range is 0 mm to 4 mm, and three-time instances are selected: 0.94 ms, 1.9 ms, and 2.5 ms. In the experiments, damage at the impact point on the backside of the specimen leads to protrusion of fiber bundles, resulting in a larger out-of-plane displacement in the central region compared to the simulation results. Additionally, fiber failure results in the loss of some speckles, causing a lack of out-of-plane displacement data at corresponding locations. Figure 6(c) compares the temperature field at 2.5 ms on the backside of the specimen, as monitored by the infrared camera at the moment of impact, with the simulation results, within a legend range of 25°C to 50°C. The comparison reveals good agreement between the experimental and simulated temperature fields, with the temperature rise localized in the central area on the specimen's backside. In both cases, the red areas indicating a higher temperature rise are due to fiber fractures, while the green areas, signifying a lower temperature increase, result from matrix cracking. The temperature distribution exhibits clear characteristics of the braided structure. In summary, the alignment of experimental data with simulation results across mechanical response curves, out-ofplane displacement contour maps, and temperature fields affirms the effectiveness of the proposed material constitutive model and the finite element model in accurately replicating low-velocity impact test scenarios.

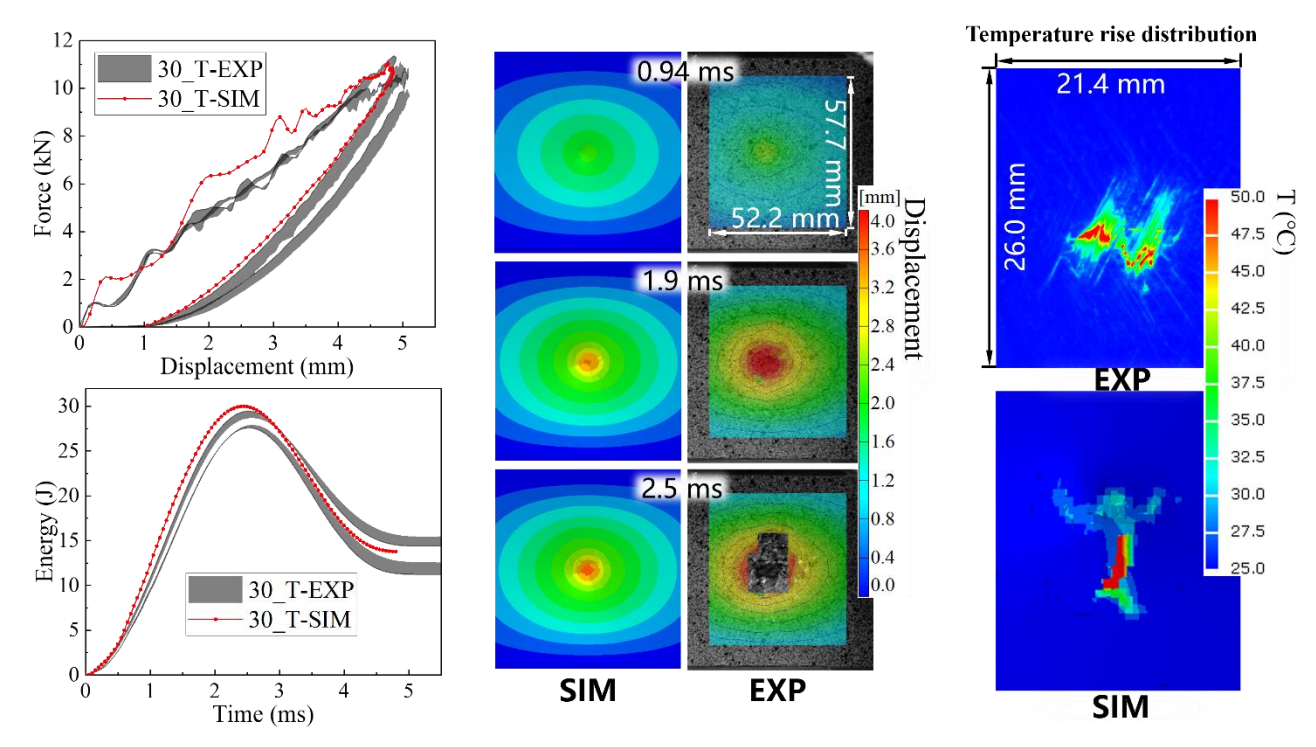


Figure 6 – Comparison of experimental and simulation results for a transverse specimen under a 30-J low-velocity impact;

Figure 7 displays the out-of-plane deformation contour map of a target plate impacted at a velocity of 89.6 m/s. The experimental out-of-plane displacement contour is slightly larger than the simulation results. In the experiments, the loss of speckles due to damage in the central area on the backside of the target plate results in missing displacement data, whereas in the simulation, areas of prominent out-of-plane displacement are also present due to fiber damage. Overall, the agreement between the experimental and simulation results is quite good, indicating that the mesoscale model can accurately simulate the overall mechanical response of the target plate in the experiments. Additionally, the Cscan delamination damage contours align closely in size with the intralaminar interface damage contours, with the interlaminar interface damage contours being slightly larger than the intralaminar ones. This is primarily due to the restriction of damage propagation at the intralaminar interfaces by the braided fiber bundles. The consistency between the experimental and simulation delamination damage contours suggests that the finite element model can replicate the internal damage conditions of the specimens in the experiments. Both the experiments and simulations indicate that the majority of the temperature rise areas are around 80°C, with small areas in the middle reaching about 100°C, mainly concentrated in the region where the projectile impacts the target plate. The destruction of the target plate's composite materials (fiber bundle fracture, matrix damage) is the primary cause of the temperature rise effect.

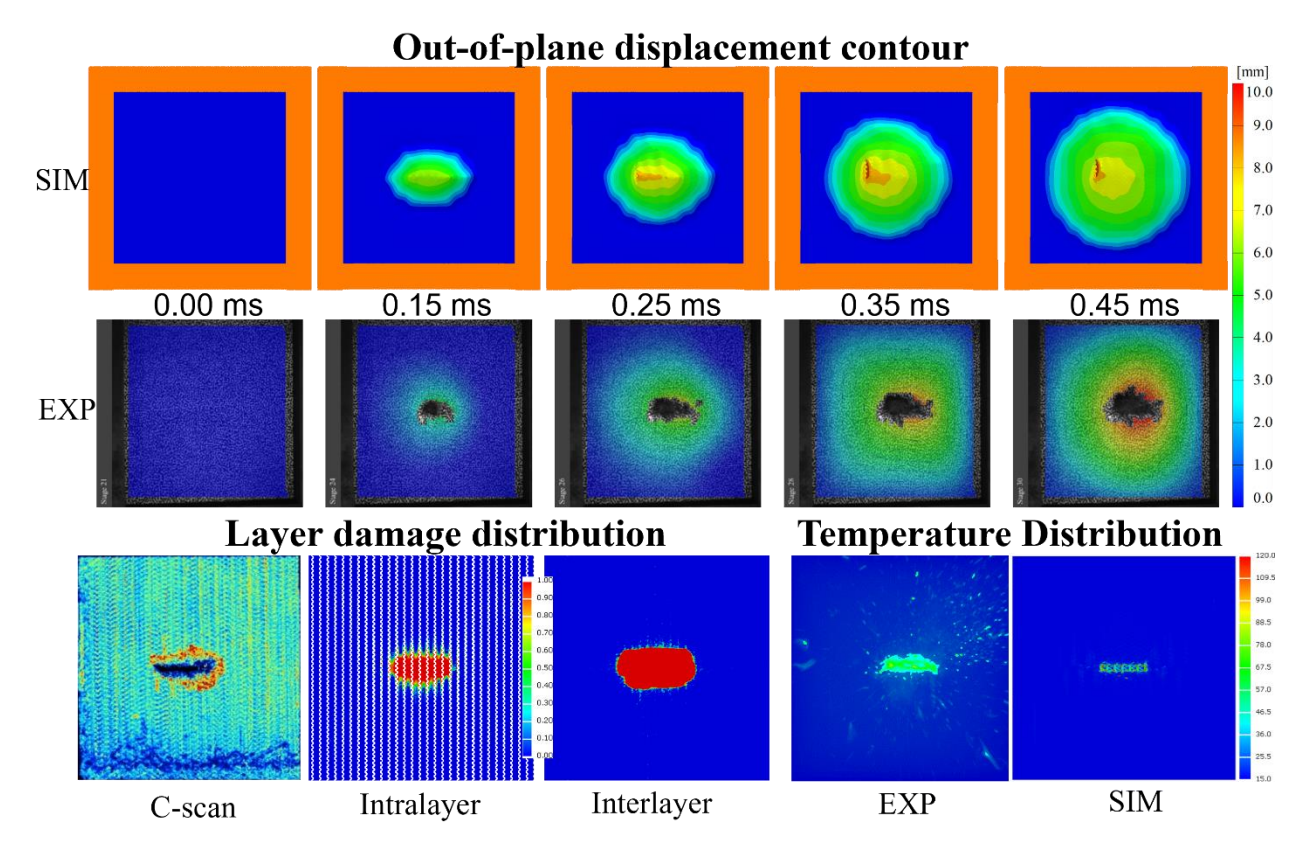


Figure 7 – Comparison between test and simulation results for high-velocity impact (89.6 m/s);

5. Conclusions

This study focuses on 2DTBC and has conducted a comprehensive series of experiments leveraging infrared thermography, including quasi-static tension, low-velocity impact, and high-velocity impact tests. These experiments have produced valuable thermal response data, coupled with geometric configurations and optical imaging, that accurately reflect the correlation between temperature rise behavior and deformation/damage mechanisms. Additionally, a rate-dependent thermomechanical coupled constitutive model for the braided composite constituents (matrix and fiber bundles) and a mesoscale finite element model for 2DTBC have been developed. Simulation analyses under quasi-static, low-velocity, and high-speed impact loading conditions were performed to elucidate the coupling effects between mechanical responses and temperature rise phenomena, revealing the underlying mechanisms governing temperature rise in braided composite materials and its influence on the overall mechanical response. The experimental and numerical integrated study adopted in this study has enabled a comprehensive understanding of the thermomechanical behavior of 2DTBC under various loading conditions, providing insights into the intricate mechanism between temperature, deformation, and damage evolution in these advanced composite materials.

Contact Author Email Address

E-mail: chaozhang@nwpu.edu.cn

Copyright Statement

The authors confirm that they, and/or their company or organization, hold copyright on all of the original material included in this paper. The authors also confirm that they have obtained permission, from the copyright holder of any third party material included in this paper, to publish it as part of their paper. The authors confirm that they give permission, or have obtained permission from the copyright holder of this paper, for the publication and distribution of this paper as part of the ICAS proceedings or as individual off-prints from the proceedings.

References

- [1] Pan Z, Zhao Q, Wei Q, et al. Heat treatment on the multiple-impact mechanical responses and damage behaviors of 3D and 2D woven GF/PP/epoxy composites. Thin-Walled Structures, 2023, 183: 110415.
- [2] Liu D, Chen P, Su J, et al. Compression properties of unidirectional over-braided multilayer composites. Composites Science and Technology, 2022, 230: 109791.
- [3] Yu J, Pan Z, Cai Q, et al. Open hole tensile behavior of plain woven carbon/glass hybrid composites. International Journal of Mechanical Sciences, 2023, 246: 108142.
- [4] Tuo H, Lu Z, Ma X, et al. Damage and failure mechanism of thin composite laminates under low-velocity impact and compression-after-impact loading conditions. Composites Part B: Engineering, 2019, 163: 642-654.
- [5] Maierhofer C, Krankenhagen R, Röllig M. Application of thermographic testing for the characterization of impact damage during and after impact load. Composites Part B: Engineering, 2019, 173: 106899.
- [6] Johnston J P, Pereira J M, Ruggeri C R, et al. High-speed infrared thermal imaging during ballistic impact of triaxially braided composites. Journal of Composite Materials, 2018, 52(25): 3549-3562.
- [7] Pan Z, Wu Z, Xiong J. High-speed infrared imaging and mesostructural analysis of localized temperature rise in damage and failure behavior of 3-D braided carbon/epoxy composite subjected to high strain-rate compression. Polymer Testing, 2019, 80: 106151.
- [8] Pan Z, Wu Z, Xiong J. Localized temperature rise as a novel indication in damage and failure behavior of biaxial non-crimp fabric reinforced polymer composite subjected to impulsive compression. Aerospace Science and Technology, 2020, 103: 105885.
- [9] Li Z, Lambros J. Dynamic thermomechanical behavior of fiber reinforced composites. Composites Part A: Applied Science and Manufacturing, 2000, 31(6): 537-547.
- [10] Pournoori N, Soares G C, Lukić B, et al. In situ damage characterization of CFRP under compression using high-speed optical, infrared and synchrotron X-ray phase-contrast imaging. Composites Part A: Applied Science and Manufacturing, 2023, 175: 107766.
- [11] Pournoori N, Soares G C, Orell O, et al. Adiabatic heating and damage onset in a pultruded glass fiber reinforced composite under compressive loading at different strain rates. International Journal of Impact Engineering, 2021, 147: 103728.
- [12] Papantonakis M R, Furstenberg R, Nguyen V, et al. Infrared imaging analysis of ballistic impacts of composite armor materials. Thermosense: Thermal Infrared Applications XXXVI. SPIE, 2014, 9105: 58-65.
- [13] Marcotte F, Ouellet S, Farley V. Analysis of the ballistic impact response of a composite material using FAST Infrared Imagery. Thermosense: Thermal Infrared Applications XXXV. SPIE, 2013, 8705: 66-73.
- [14] Pan Z, Gu B, Sun B. Longitudinal compressive behaviour of 3D braided composite under various temperatures and strain rates. Applied Physics A, 2015, 118: 1315-1337.
- [15] Pan Z, Gu B, Sun B. Thermo-mechanical behaviors of 3-D braided composite material subject to high strain rate compressions under different temperatures. Mechanics of Advanced Materials and Structures, 2016, 23(4): 385-401.
- [16] Zhang W, Gu B, Sun B. Thermal-mechanical coupling modeling of 3D braided composite under impact compression loading and high temperature field. Composites Science and Technology, 2017, 140: 73-88.
- [17] Chen Z, Wang Q, Zhang Y, et al. Failure mechanism of thermo-mechanical coupling of 3D braided composites with different thickness under high strain-rate punch shear loading. Composite Structures, 2022, 279: 114826.
- [18] Zhao Z, Liu P, Chen C, et al. Modeling the transverse tensile and compressive failure behavior of triaxially braided composites. Composites Science and Technology, 2019, 172: 96-107.
- [19] ASTM International. ASTM D7136: Standard Test Method for Measuring the Damage Resistance of a Fiber-Reinforced Polymer Matrix Composite to a Drop-Weight Impact Event. ASTM International, West Conshohocken, Pa., USA, 2020.
- [20] Dassault Systèmes Simulia Corporation. Abaqus analysis user's manual. Abaqus 2020 Documentation, Dassault Systèmes Simulia Corporation, Providence, R.I., USA, 2020.